International Research Journal of Engineering and Technology (IRJET) e-ISSN: 2395-0056
Volume: 06 Issue: 04 | Apr 2019 www.irjet.net p-ISSN: 2395-0072

Study on the Feature of Cavitation Bubbles in Hydraulic Valve by using a Single Camera and 6 Mirrors

Chan-Il Pak[1], Chang-Hyon Rim[2], Un-Jin Pak[3], Ok-Chol Song[1], Hui-Gan Kim[1]

[1]Information Centre, Kim Chaek University of Technology, Pyongyang 950003, D.P.R.Korea
[2]Department of Machine Engineering, Kim Chaek University of Technology, Pyongyang 950003, D.P.R.Korea
[3]Department of Automatic Engineering, Kim Chaek University of Technology, Pyongyang 950003, D.P.R.Korea

---

Abstract - *Three-dimensional features of bubbles are of great importance to understand the flow mechanism in cavitation bubbly flows. It is very efficient to study the 3D features of bubbles by using a virtual stereo sensor including a single camera and 4 mirrors proposed previously. But this method is not suitable to consider the space with an opaque object. Therefore, in this paper, one sensor with 6 mirrors is proposed for the consideration of the feature parameters of bubbles generated by cavitation phenomenon in a hydraulic valve with an opaque object. And, one algorithm is proposed to extract the 3D features and size of bubbles from a video file. For the effectiveness verification of the proposed method, the 3D features of the motion trajectory and velocity of bubbles in the hydraulic valve are considered. The experiments demonstrated the effectiveness of this method for the investigation of 3D features of cavitation bubbles in the hydraulic valve.*

Key Words: Gas-liquid two-phase flow, Cavitation bubbles, Virtual stereo vision, 3D measurement

1. Introduction

The cavitation is a typical flow phenomenon, which is easily seen in many fields, such as fluid machine, power and chemical industry. The study on the mechanism of flow often requires describing the size, shape, trajectory and velocity of bubbles generated by the cavitation accurately. Therefore, the exploring of morphology and 3D motion features of the cavitation bubble is the first issue need to be solved.

The main detecting methods of the characteristic parameters of bubbles can be divided into the invasive and noninvasive methods currently. The invasive methods use the optical fibre probe [1], and the noninvasive methods include PIV (Particle Image Velocimetry), PTV (Particle Tracking Velocimetry), PT (Process Tomography) and so on [2-3]. As the noninvasive methods are noncontact and have no interference to the flow field, they play an important role in studying the gas-liquid two phase flows. In particular, the high-speed photography technology [4] is one of the most widely used methods, due to the easiness of implementation and no interference to the parameter measurement in the flow field.

In the high-speed photography technology, the high speed camera [5-9], MRI (Magnetic Resonance) [10-11], Phase Doppler Anemometry [12] and laser [13], are used to take images of gas-liquid two phase flow. The method using the high speed camera is largely divided into two types: the method using multiple cameras and the other one using a single camera and mirrors. The study on the method using a single camera and 4 mirrors has begun in early 1990, and this is the effective method with low measurement cost. This method is useful to study the bubble flow inside a transparent object, but not suitable for the case of hydraulic valve with an opaque object in it.

The main point of the virtual stereo vision technique is the stereo and motion matching of bubbles. The early researchers matched a given bubble in the left and right images with naked eyes based on the approximately same vertical coordinates, and later some methods for the stereo matching were proposed [14]. The motion matching is also an indispensable element to reconstruct the bubble trajectories, and a correct result of stereo matching is a guarantee of the motion matching and 3D reconstruction. Some researchers studied the motion matching [15]. In the literature [16], a multi-variable constrained threshold matching method was proposed. This method set a threshold of the ordinate D-value and the projection height D-value of bubbles in the left and right images to reduce the searching area, and then the bubble was affirmed by fusion of the epipolar line minimum distance constraint and the reverse epipolar line constraint. Then, a 3D polar coordinate homonymy correlation algorithm was proposed after combining the 3D polar coordinate system with the homonymy unit.

In this paper, virtual stereo vision measurement system using a single camera and 6 mirrors is developed to consider the 3D features of cavitation bubbles inside the hydraulic valve, based on the investigation of the above-mentioned literature. Then, one algorithm is proposed to extract the 3D features and size of cavitation bubbles from the obtained video file. The 3D features and size of cavitation bubbles inside the hydraulic valve is considered by using the proposed method. The experiments show the superiority of the proposed method over previous methods.

The paper is organized as follows. Section 2 introduces the virtual stereo vision system with 6 mirrors using an existing single camera and 4 mirrors. In section 3, the virtual stereo vision system and the algorithm for the extraction of features for the measurement of cavitation bubbles inside the hydraulic valve are developed. Section 4 describes the

experiments for the measurement of cavitation bubbles 3D features and size by using the proposed method. In section 5, the experimental results and the future research are introduced.

2. 3D measurement model of virtual stereo vision

2.1 Camera model

Camera image is constructed by the perspective projection of space points into the 2D image plane. The perspective projection model of the camera in the virtual stereo vision sensor is shown in Fig.1. Where on is the center of the camera image plane π, o_c is the projection center of the camera and z_c is the optical axis of the camera lens. The relative coordinate frames are defined as follows: $o_c x_c y_c z_c$ is the 3D camera coordinate frame, $o_u x_u y_u$ is the 2D image plane coordinate frame and $o_w x_w y_w z_w$ is the 3D world coordinate frame.

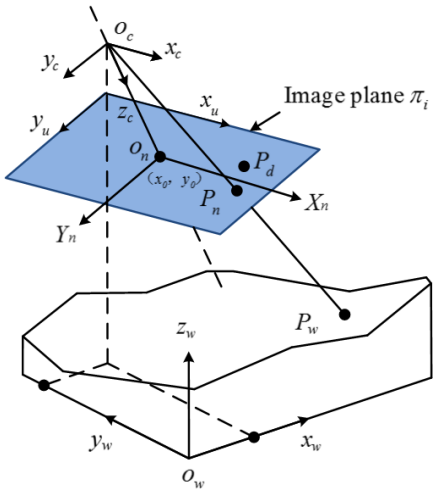

Fig.1: Perspective projection model of camera

Given one point P_w in 3D space, its homogeneous coordinate in $o_w x_w y_w z_w$ is represented by $\bar{P}_w = (x_w \; y_w \; z_w \; 1)^T$. P_n is the ideal projection of P_w in the camera image plane and P_d is the real projection, because of lens distortion. Similarly, $\tilde{p}_u = (x_u \; y_u \; 1)^T$ can be used to denote P_n's homogeneous coordinate in $o_u x_u y_u$. According to the pinhole perspective projection theory of camera, the relationship between a 3D point and its image projection can be given by

$$s\tilde{p}_u = A\begin{bmatrix} R & T \end{bmatrix}\tilde{P}_w \tag{1}$$

where $A = \begin{bmatrix} f_x & 0 & x_0 \\ 0 & f_y & y_0 \\ 0 & 0 & 1 \end{bmatrix}$ and s is an any scale factor.

A is called the camera intrinsic parameter matrix, f_x, f_y the effective focal length in pixels in the x and y directions respectively, and x_0; y_0 the coordinate of the principle point. $\begin{bmatrix} R & T \end{bmatrix}$ is the camera extrinsic parameter converting the 3D world coordinate into the camera coordinate. R is the 3×3 orthogonal rotation matrix, T the 3×1 translation vector.

As the optical system with a camera has lens distortion, it should be considered in 3D measurement. The radial lens distortion can be given by

$$\begin{bmatrix} x_r \\ y_r \end{bmatrix} = (1 + k_1 r_u^2 + k_2 r_u^4 + k_3 r_u^6)\begin{bmatrix} x_u \\ y_u \end{bmatrix} \tag{2}$$

where r_u is the distance from the principal point to the projection one in the absence of distortion, $r_u^2 = x_u^2 + y_u^2$, and k_1, k_2 and k_3 are the coefficients of lens. But, in reality, only k_1 and k_2 are considered. The tangential lens distortion is given by

$$\begin{bmatrix} x_t \\ y_t \end{bmatrix} = \begin{bmatrix} 2p_1 x_u y_u + p_2(r_u^2 + 2x_u^2) \\ p_1(r_u^2 + 2y_u^2) + 2p_2 x_u y_u \end{bmatrix} \tag{3}$$

where p_1 and p_2 are the coefficients of tangential lens distortion. Therefore, in the presence of distortion, the actual projection coordinate can be obtained as follows:

$$\begin{bmatrix} x_d \\ y_d \end{bmatrix} = (1 + k_1 r_u^2 + k_2 r_u^4 + k_3 r_u^6)\begin{bmatrix} x_u \\ y_u \end{bmatrix} + \begin{bmatrix} 2p_1 x_u y_u + p_2(r_u^2 + 2x_u^2) \\ p_1(r_u^2 + 2y_u^2) + 2p_2 x_u y_u \end{bmatrix} \tag{4}$$

In the above equations, all the intrinsic and extrinsic parameters of the camera are obtained when the camera is calibrated. However, because of the nonlinear nature of the camera model due to lens distortion, there always exists the inconsistency between the estimated coordinate and the coordinates of actually measured feature points. Thus an iterative optimization algorithm is used to reduce measurement errors between the model and observations.

The optimization objective function can be obtained as follows:

$$F(x)=\sum_{i=0}^{n}((X_i-x_i)^2+(Y_i-y_i)^2) \quad (5)$$

where (x_i, y_i) is the real measured image coordinate, and (X_i, Y_i) is the coordinate estimated by the camera model. The intrinsic and extrinsic parameters of the camera due to lens distortion are estimated by the least squares fitting algorithm [17].

2.2 Calibration of the virtual stereo vision sensor

A 3D measurement model of the virtual vision sensor combined with a left camera coordinate system and a right camera coordinate system is shown in Fig.2.

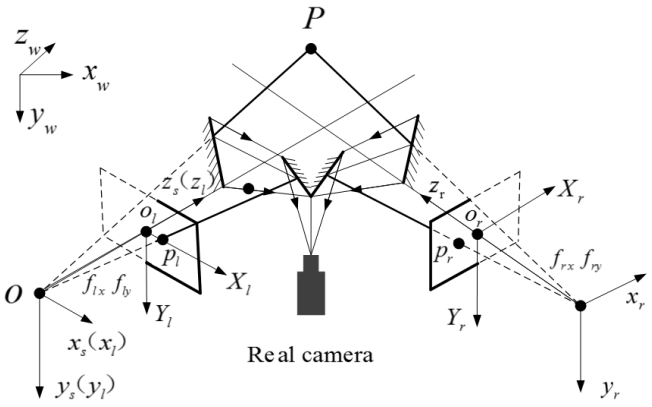

Fig.2: 3D measurement model

where, the relative coordinate frames can be obtained as follows.: $o_w x_w y_w z_w$ represents the 3D world coordinate frame, $o_l x_l y_l z_l$ is the 3D coordinate frame of the left virtual camera, $o_l x_l y_l$ its corresponding image plane coordinate frame, $o_r x_r y_r z_r$ the 3D coordinate frame of the right virtual camera and $o_r x_r y_r$ its corresponding 2D image plane coordinate frame. $ox_s y_s z_s$ is the sensor measurement coordinate frame, which overlaps with $o_l x_l y_l z_l$.

Given an arbitrary 3D point P, let $\tilde{P}_S=\begin{bmatrix}x_S & y_S & z_S & 1\end{bmatrix}^T$ be the 3D homogeneous coordinate of point P in $ox_s y_s z_s$, and $\tilde{P}_r=\begin{bmatrix}x_r & y_r & z_r & 1\end{bmatrix}^T$ be the 3D coordinate in $o_r x_r y_r z_r$. p_l, p_r are the ideal projections of P in the left and right half image planes of the camera, and their corresponding homogeneous coordinates in $o_l X_l Y_l$ and $o_r X_r Y_r$ are denoted by $\tilde{P}_l=\begin{bmatrix}X_l & Y_l & 1\end{bmatrix}^T$, $\tilde{P}_r=\begin{bmatrix}X_r & Y_r & 1\end{bmatrix}^T$. The position and orientation of the L/R virtual cameras can be defined by

$$P_r=\begin{bmatrix}R & T\end{bmatrix}\tilde{P}_S \quad (6)$$

where T is the translation matrix, R is the orthogonal rotation matrix between $ox_s y_s z_s$ and $o_r x_r y_r z_r$ expressed by equation (7) and (8).

$$T=\begin{bmatrix}t_x & t_y & t_z\end{bmatrix}^T \quad (7)$$

$$R=\begin{bmatrix}r_1 & r_2 & r_3\\ r_4 & r_5 & r_6\\ r_7 & r_8 & r_9\end{bmatrix} \quad (8)$$

According to the perspective projection model of camera, $p_l=z_s$, $p_l\tilde{p}_l=P_s$, $p_r\tilde{p}_r=P_r$.

Therefore, 3D measurement model of the virtual stereo vision sensor can be expressed as follows:

$$\begin{cases} x_S=z_S X_l \\ y_S=z_S Y_l \\ z_S=\dfrac{t_x-X_r t_z}{X_r(r_7X_l+r_8Y_l+r_9)-(r_1X_l+r_2Y_l+r_3)} \\ \quad =\dfrac{t_y-Y_r t_z}{Y_r(r_7X_l+r_8Y_l+r_9)-(r_4X_l+r_5Y_l+r_6)} \end{cases} \quad (9)$$

The accurate parameters can be estimated by the nonlinear iterative optimizing algorithm [17] and the accurate distance of feature points. According to Eq.(9), we can estimate the 3D coordinate of measured feature points if their homogeneous image coordinates, R and T are known exactly.

3. A proposed 3D measurement model using 6 mirrors

3.1 Measurement model

The proposed 3D measurement model is shown in Fig.3(a). We constructed the measurement model by adding two mirrors to the model of Fig.2 for the purpose of obtaining the images of 4 sides of one object simultaneously. The camera calibration of the proposed measurement model can be performed in the same way as one in the existing virtual stereo vision sensor. Because of the increase in the number of virtual cameras, the calculating amount of parameters for the calibration gets much bigger. Fig.3(b) shows the dimensions of the real virtual stereo vision sensor.

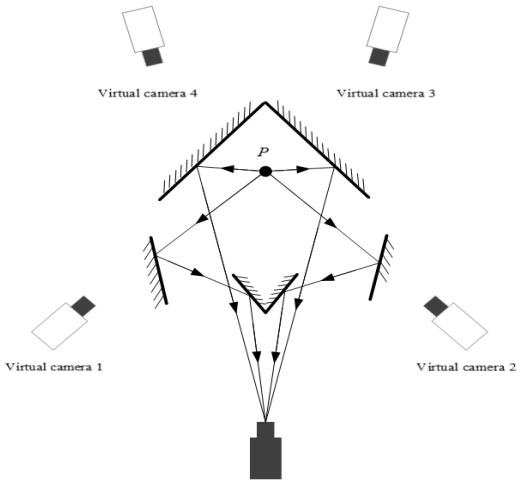

(a): 3D measurement model;

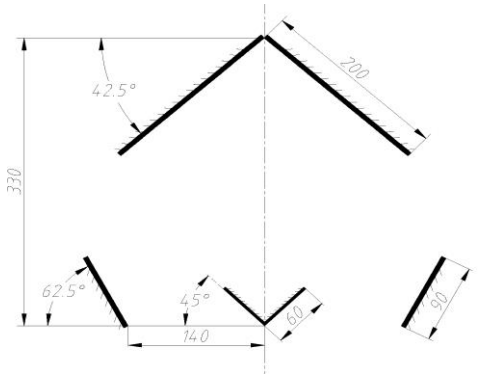

(b): Dimensions of the proposed 3D sensor;

Fig.3: A proposed 3D virtual stereo vision sensor.

3.2 Extraction of features

The result from the virtual stereo vision sensor is a true color video file, and this file is a group of images. Obtaining the feature data of bubbles from the images requires pre-processing and the process is shown in Fig.4(a). Here, the base frame (F_b) is the one before the generation of bubbles. The diameter (D) of a bubble is determined by the width (w) and height (h) of the detected area, and the center of a bubble is estimated by the detected coordinate (x_{lt}, y_{lt}), w and h (Fig.4(b)).

$$D = 0.5 \times (w + h) \tag{10}$$

$$\begin{cases} x = x_{lt} + 0.5 \times w \\ y = y_{lt} + 0.5 \times h \end{cases} \tag{11}$$

where x_{lt}, y_{lt} are the x, y coordinates of the bubble detected initially in the left-top point. The center of mass coordinates can then be used to reconstruct the 3D motion parameters of the bubbles. A bubble in any position, surely, appears in the images of over two virtual cameras and the most apparent two images of them are used in the measurement.

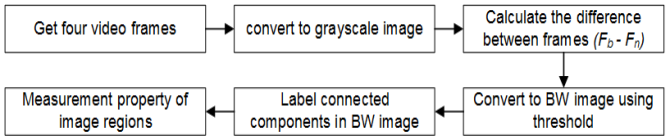

(a): Algorithm;

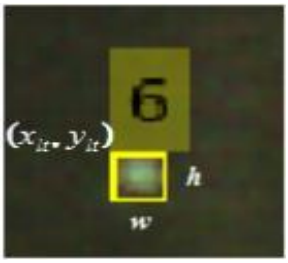

(b): Coordinate of a bubble;

Fig.4: Feature extraction algorithm and coordinate of a bubble.

3.3 3D reconstruction of motion parameters

The main motion feature parameters of a bubble includes the trajectory and velocity. Once the center coordinate of a bubble is extracted accurately by the algorithm of feature extraction and the intrinsic - extrinsic parameters of the virtual stereo vision sensor are estimated through the calibration, the 3D position of a bubble can be determined precisely. The 3D position of a bubble obtained at a certain period of time is used to reconstruct its trajectory and determine its velocity. The velocity of a bubble is obtained by the motion distance per a second. Let the coordinate of a bubble at the moment of t_0 be (x_0, y_0, z_0) and that at t_1 is (x_1, y_1, z_1), its velocity is calculated as follows.

$$\upsilon = \frac{\sqrt{(x_1 - x_0)^2 + (y_1 - y_0)^2 + (z_1 - z_0)^2}}{t_1 - t_0} \tag{12}$$

where $(t_1 - t_0)$ can be calculated by frames' number during the time and N_{fps} frames per a second.

$$\Delta t = \frac{f_1 - f_0}{N_{fps}} \tag{13}$$

4. Experiment

4.1 Experimental setup

Fig.5 shows the experimental setup using the virtual stereo vision measurement model. The experimental setup consists of an electricity control, hydraulic and visible modules. The frequency converter in the electricity control module is used to control the rotation speed of the hydraulic motor, i.e. its input pressure. The hydraulic module includes the transparent hydraulic valve for measurement, a water tank, various fluid control valves and sensors. The visible module includes the high speed camera, the proposed 3D sensor, an industrial computer and a source of light. The high speed camera (Revealer 5KF10) is capable of taking images of 1280×860 pixels at $4000f/s$ and uses the lens of 60mm Nikkor.

In the experiment, we considered the features of cavitation bubbles generated in the hydraulic valve. Closed water is used in the experiment, and the cavitation bubbles are generated by the difference between the input pressure and the output pressure of the hydraulic valve. The input pressure of water through the hydraulic valve is controlled by the frequency converter, and its output pressure is controlled by the space between the valve seat and valve core. The smaller the space, the larger the difference between the input and output pressures and the generation probability of the cavitation bubble.

4.2 Calibration and 3D reconstruction

Before the measurement of the 3D features of cavitation bubbles, the generating bubble number and the size distribution, the proposed virtual stereo vision sensor should be calibrated. For the calibration, a double-faced calibration reference object is used, and according to the perspective projection model of camera the intrinsic parameters of 4 virtual cameras are measured.

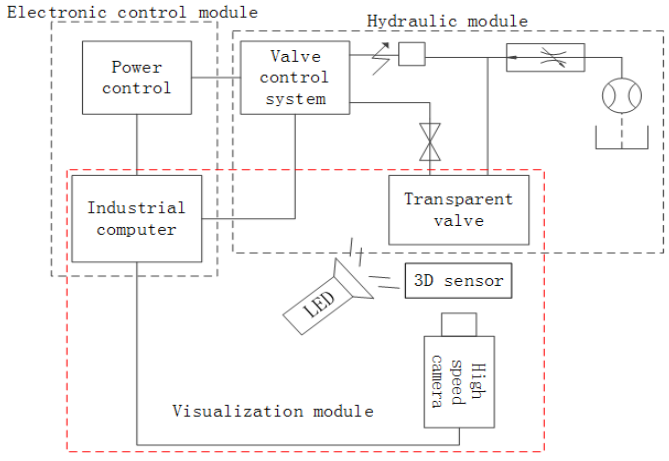

(a): Block diagram;

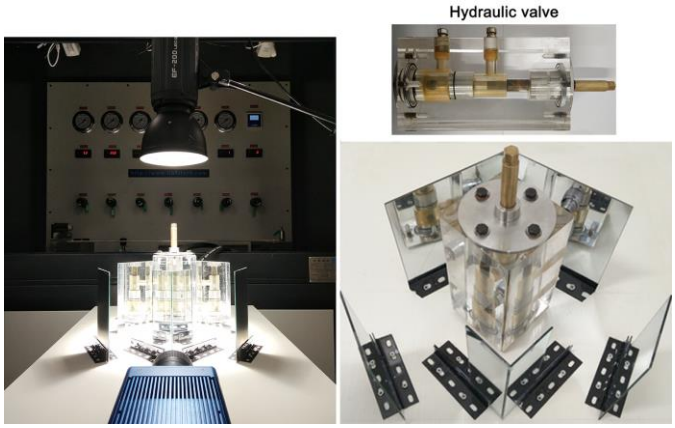

(b): Experimental setup;

Fig.5: Block diagram and experimental setup.

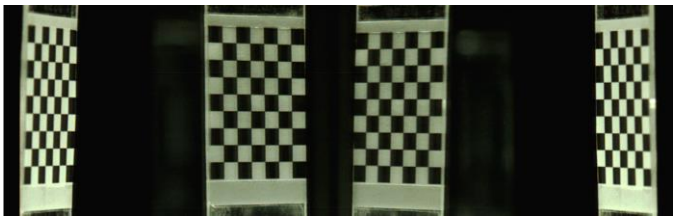

(a): Calibration image;

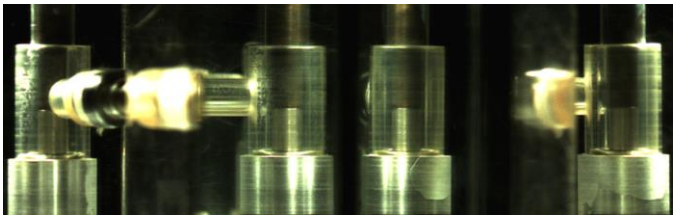

(b): Camera image;

Fig.6: Calibration process.

The virtual camera 1 intrinsic parameters are

f_x = 5514.17855 pixels, f_y = 5524.46751 pixels,

u_0 = 671.53442 pixels, v_0 = 492.23142 pixels,

k_1 = 0.32022, k_2 = -0.45861,

p_1 = 0.00069, p_2 = -0.00089.

The virtual camera 2 intrinsic parameters are

f_x = 5565.16765 pixels, f_y = 5577.42417 pixels,

u_0 = 667.19514 pixels, v_0 = 421.93592 pixels,

k_1 = 0.16770, k_2 = -0.23900,

p_1 = 0.00024, p_2 = -0.00050.

The virtual camera 3 intrinsic parameters are

f_x = 4950.74783 pixels, f_y = 4840.37332 pixels,

u_0 = 663.40892 pixels, v_0 = 430.01220 pixels,
k_1 = 0.13188, k_2 = -0.37245,
p_1 = 0.00054, p_2 = -0.00021.

The virtual camera 4 intrinsic parameters are

f_x = 4910.74783 pixels, f_y = 4710.37332 pixels,
u_0 = 683.41245 pixels, v_0 = 430.51424 pixels,
k_1 = 0.25370, k_2 = -0.30036,
p_1 = 0.00012, p_2 = -0.00160.

Then, basing on the mathematical model of the virtual stereo vision sensor, the translation and orthogonal rotation matrix between two virtual cameras are estimated as follows.

The extrinsic parameters between the virtual camera 1 and 2 are

$$R_{12} = \begin{bmatrix} 0.2512 & 0.0943 & 0.9633 \\ 0.1107 & 0.9951 & -0.0682 \\ -0.9616 & -0.0895 & 0.2595 \end{bmatrix}$$

$$T_{12} = \begin{bmatrix} -602.5004 & 12.0292 & 395.2692 \end{bmatrix}^T$$

The extrinsic parameters between the virtual camera 2 and 3 are

$$R_{23} = \begin{bmatrix} 0.1084 & -0.3486 & 0.9310 \\ 0.8480 & 0.5212 & -0.0964 \\ -0.5188 & 0.7790 & -0.3521 \end{bmatrix}$$

$$T_{23} = \begin{bmatrix} -626.1676 & 28.1869 & 680.9081 \end{bmatrix}^T$$

The extrinsic parameters between the virtual camera 3 and 4 are

$$R_{34} = \begin{bmatrix} -0.8667 & 0.0024 & 0.4988 \\ 0.0089 & 0.9999 & 0.0107 \\ -0.4988 & 0.0137 & -0.8666 \end{bmatrix}$$

$$T_{34} = \begin{bmatrix} -289.7553 & -18.1662 & 676.9837 \end{bmatrix}^T$$

The extrinsic parameters between the virtual camera 4 and 1 are

$$R_{41} = \begin{bmatrix} 0.1719 & -0.0038 & 0.9851 \\ -0.0003 & 1.0000 & 0.0039 \\ -0.9851 & -0.0010 & 0.1719 \end{bmatrix}$$

$$T_{41} = \begin{bmatrix} -670.9189 & -0.8545 & 633.9629 \end{bmatrix}^T$$

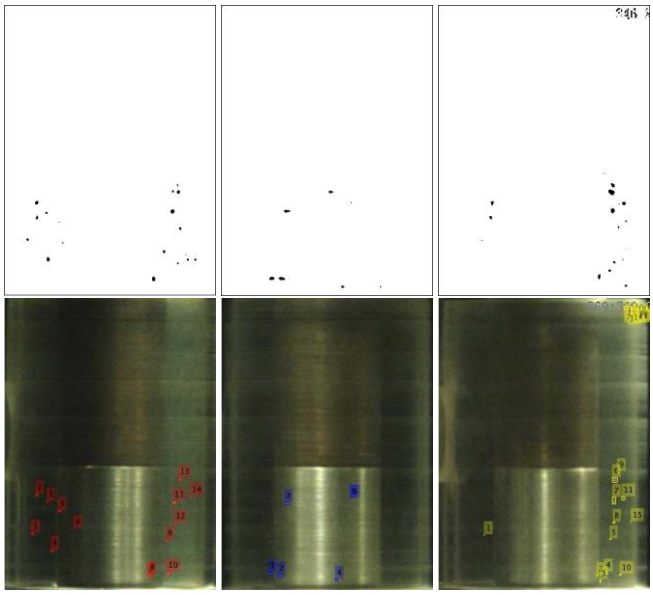

(a): Virtual camera 1; **(b):** Virtual camera 2; **(c):** Virtual camera 3;

Fig.7: Bubble extraction results.

Fig.7 shows the extraction results of bubbles obtained by the feature extraction algorithm. Based on the intrinsic - extrinsic parameters of camera and the center coordinate of a bubble obtained through the above measurement, the 3D trajectory of a cavitation bubble is reconstructed based on the mathematical model of the virtual stereo vision sensor. In the experiment, a bubble in consideration surely is captured by any two virtual cameras, so it has two pairs of distorted coordinates. Based on the distorted coordinates, a relative one is obtained, and then, by using rotation and translation matrix of virtual cameras, the coordinate is converted to the relative one with the camera 2 as the reference system. Therefore, the amount of calculation increases. Fig.8(a) shows the trajectory of a reconstructed bubbles, Fig.8(b) shows the velocity vector graph of a bubble obtained by the equation(12) and (13).

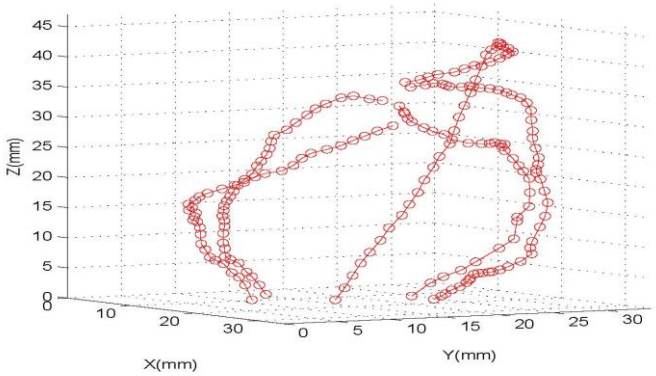

(a): Trajectory of a bubble;

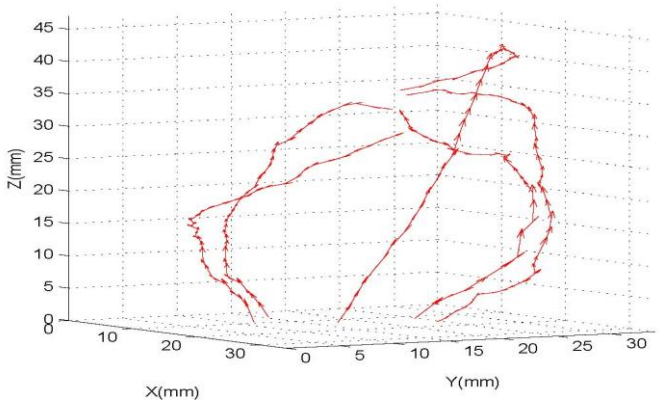

(b): Velocity vector of a bubble;

Fig.8: Experimental results.

4.3 Analysis of experimental results

Fig.9(a) shows the size variation graph of a bubble. As seen in Fig.9(a), the bubble generated by the cavitation phenomenon rapidly grows bigger until the inner and outer pressures are the same, once they are the same, its size does not change. According to the theory, when the inner pressure of a cavitation bubble becomes bigger than its outer one, the bubble breaks and vanishes, and it causes the corrosion of mechanical devices. But, as the considered space $(34mm(r)\times 28.5mm(h))$ in the experiment is small and the motion velocity of liquid is very fast, the bubble goes beyond the space before breaking.

Fig.9(b) shows the size distribution graph of the bubbles generated by the cavitation phenomenon when the inner pressure $P_i = 6.55bar$ and the outer pressure $P_0 = 1bar$. As seen in Fig.9(b), the size distribution of a bubble is similar to the gaussian distribution.

The experiments demonstrated that the proposed method is suitable for the consideration of the inside of space with an opaque subject, especially, for that of the features of cavitation bubbles in hydraulic valve.

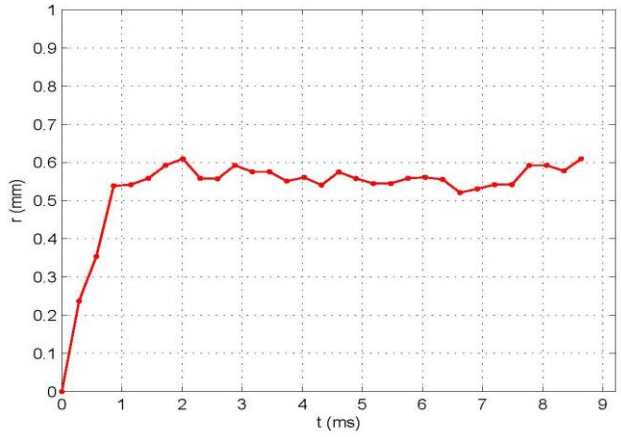

(a): Size variation;

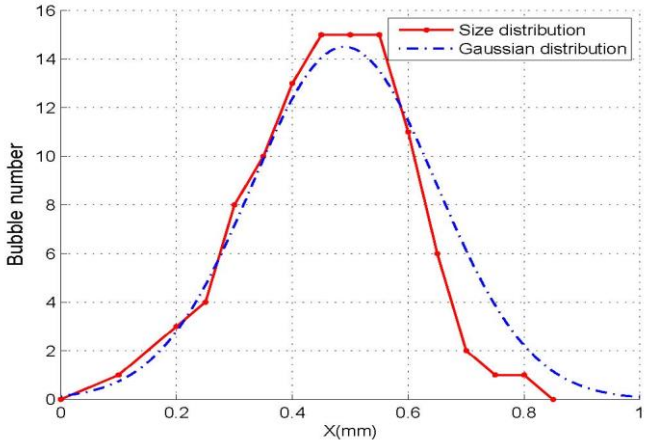

(b): Size distribution;

Fig.9: Size variation and distribution graph of a bubble.

5. Conclusion and future research work

In this paper, firstly, based on the reference investigation, one virtual stereo vision sensor using 6 mirrors for the measurement of bubble features generated by the cavitation phenomenon was proposed. Secondly, an algorithm for the extraction of bubble features from the video file obtained by the proposed sensor was introduced. Thirdly, the experiments demonstrated that the sensor had a good performance in the measurement of bubbles generated in the hydraulic valve. The future research work is to make the database of feature data of the cavitation bubbles according to the design characteristics of hydraulic valve, based on the proposed method. This database can be used as the basic data in the intelligent cooperative design system.

Acknowledgment

I would like to take the opportunity to express my hearted gratitude to all those who make a contribution to the completion of my article.

References

[1] S. Guet, S. Luther, G. Ooms, Bubble shape and orientation determination with a four-point optical fibre probe, Experimental Thermal & Fluid Science, 29(7) (2003) 803-812.

[2] M. Monica, JH. Cushman, A. Cenedese, Application of photogrammetric 3D-PTV technique to track particles in porous media, Transport in Porous Media. 79(1) (2009) 43-65.

[3] PM. Bardet, PF. Peterson, mer. Sava, Split-screen single-camera stereoscopic PIV application to a turbulent confined swirling layer with free surface, Experiments in Fluids. 49(2) (2010) 513-524.

[4] E. Rathakrishnan, Visualization of the flow field around a flat plate, IEEE Instrumentation & Measurement Magazine. 15(6) (2012) 8-12.

[5] M. Wu, M. Gharib, Experimental studies on the shape and path of small air bubbles rising in clean water, Physics of Fluids. 14(7) (2002) L49-L52.

[6] A. Vazquez, RM. Sanchez, E. Salinas-Rodrguez, A. Soria, R. Manasseh, A look at three measurement techniques for bubble size determination, Experimental Thermal & Fluid Science. 30(1) (2005) 49-57.

[7] M. Maldonado, JJ. Quinn, CO. Gomez, JA. Finch, An experimental study examining the relationship between bubble shape and rise velocity, Chemical Engineering Science. 98(29) (2013) 711.

[8] W. Kracht, JA. Finch, Effect of frother on initial bubble shape and velocity, International Journal of Mineral Processing. 94(34) (2010) 115-120.

[9] V. Tesa, Shape oscillation of microbubbles, Chemical Engineering Journal. 235(1) (2014) 368-378.

[10] AB. Tayler, DJ. Holland, AJ. Sederman, LF. Gladden, Applications of ultra-fast MRI to high voidage bubbly flow: Measurement of bubble size distributions, interfacial area and hydrodynamics, Chemical Engineering Science. 71(71) (2012) 468483.

[11] DJ. Holland, A. Blake, AB. Tayler, AJ. Sederman, LF. Gladden, Bubble size measurement using Bayesian magnetic resonance, Chemical Engineering Science. 84(52) (2012) 735-745.

[12] G. Brenn, H. Braeske, F. Durst, Investigation of the unsteady two-phase flow with small bubbles in a model bubble column using phase-Doppler anemometry, Chemical Engineering Science. 57(24) (2002) 5143-5159.

[13] G. Lacagnina, S. Grizzi, M. Falchi, FD. Felice, GP. Romano, Simultaneous size and velocity measurements of cavitating microbubbles using interferometric laser imaging, Experiments in Fluids. 50(4) (2011) 1153-1167.

[14] JC. Kent, AR. Eaton, Stereo photography of neutral density He-filled bubbles for 3-D fluid motion studies in an engine cylinder, Applied Optics. 21(5) (1982) 904-12.

[15] R. Luo, Q. Song, XY. Yang, Z. Wang, A three-dimensional photographic method for measurement of phase distribution in dilute bubble flow, Experiments in Fluids. 32(1) (2002) 116-120.

[16] T. Xue, L. Qu, B. Wu, Matching and 3-D Reconstruction of Multibubbles Based on Virtual Stereo Vision, IEEE Transactions on Instrumentation & Measurement. 63(6) (2014) 1639-1647.

[17] JJ. Mor, The Levenberg-Marquardt algorithm: Implementation and theory, Lecture Notes in Mathematics. 630 (1978) 105-116.

BIOGRAPHIES

Chan-Il Pak received the B.SC and M.SC degrees in computer engineering from Kim Chaek University of Technology, DPR of Korea in 1999 and 2003, respectively. Currently, I is a professor in information center at Kim Chaek University of Technology.

Chang-Hyon Rim, born in 1979, is currently a PhD candidate at Harbin Institute of Technology, China. I received my bachelor degree from Kim Chaek University, DPR of Korea, in 2006. My research interests include Machine Engineering and Manufacturing.

Un-Jin Pak, born in 1980, is currently a PhD candidate at Harbin Institute of Technology, China. I received my bachelor degree from Kim Chaek University, DPR of Korea, in 2007. My research interests include Automatic Control Engineering.